Calorimetric Efficiency Measurements of Supercapacitors and Lithium-Ion Batteries

Antti Virtanen, Hannu Haapala, Saara Hännikäinen, Tuomas Muhonen and Heikki Tuusa
Tampere University of Technology
Department of Electrical Energy Engineering
Tampere, Finland
Email: antti.a.virtanen@tut.fi

***Abstract*—This paper presents efficiency measurements for a 125 V/63 F supercapacitor module (SC) and a 96 V/90 Ah lithium-ion (li-ion) battery system as a function of charge-discharge current frequency. The result would be useful in the design of efficient power flow control in systems using SCs and li-ion batteries as parallel energy storages, and offers a possibility to predict energy storage power losses from the frequency spectrum of the energy storage current. In order to obtain accurate measurement results a calorimetric test setup has been built. In addition the li-ion battery efficiency is analyzed according to draft standard ISO 12405-1 and with a small scale straddle carrier laboratory drive. The calorimetric measurements indicate that frequency has only a minor impact on the energy storage efficiencies, but the efficiency of the SC is approximately 3 % better than that of the li-ion battery system. The standard measurements and straddle carrier measurements indicate an even greater difference in li-ion battery efficiency in comparison to the SC. Hence, in parallel SC and li-ion battery energy storage systems the control of power flow should be arranged so that the SC is utilized as much as possible.**

I. INTRODUCTION

Electric energy storage and reutilization, used in hybridization of diesel powered vehicles and heavy-duty work machines (HWM), offers an opportunity to improve the fuel efficiency and reduce the emissions in different applications [1–4]. Typically a HWM operates with a repetitive load pattern in which charging and discharging the energy storage occurs within a recognizable frequency range. Eg. the typical charge-discharge frequencies for the energy storage in a straddle carrier or forklift truck application are close to 0 Hz, but in a forestry harvester or a stone crusher frequencies up to 5 Hz have been recorded [3], [5].

This paper investigates the efficiencies of two possible energy storage solutions in HWM applications as a function of charge-discharge current frequency. The types of energy storage studied are a Maxwell BMOD0063 P125 V/63 F heavy-duty supercapacitor module (SC) and a K2 96 V/ 90 Ah lithium-ion (li-ion) battery system comprising of 30 pcs of LFP300HES Energy Modules. The battery pack includes a battery management system (BMS) for cell voltage balancing and for monitoring the state of charge (SOC), temperature, voltage and current. The energy storages are presented in Figs. 1 and 2 respectively. Table I presents fundamental characteristics of the energy storages according to the manufacturers' datasheets.

In order to accurately measure the efficiencies, a calorimetric test setup has been built. The aim of the measurements is to ascertain if there is a distinct boundary frequency, after which one energy storage is clearly more energy efficient than the other. The result would be useful in designing efficient control of energy storage power flow in

Figure 1. Maxwell BMOD0063 P125 V/63 F heavy-duty supercapacitor module.

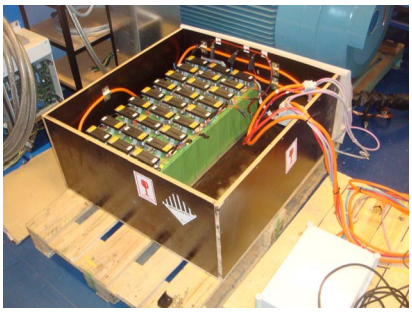

Figure 2. K2 96 V/ 90 Ah li-ion battery system of 30 pcs of LFP300HES Energy Modules.

TABLE I. FUNDAMENTAL CHARACTERISTICS OF ENERGY STORAGES

Maxwell BMOD0063 P125 V/ 63 F supercapacitor module	
Nominal capacitance	63 F + 20 %/ -0%
Rated voltage	125 V
Maximum continuous current	150 A
Available energy	101.7 Wh
Equivalent series resistance $R_{ESR,SC}$	18 mΩ
K2 LFP300HES 96 V/ 90 Ah lithium-ion battery system	
Nominal capacity @ C/5	90 Ah
Rated voltage @ C/5	96 V
Maximum continuous current	300 A, discharge
Available energy	8640 Wh
Internal impedance @ 1 kHz, AC	< 150 mΩ

systems using multiple parallel energy storage systems, as depicted in [4], [6–8]. By knowing the frequency dependence of the energy storage efficiency and equivalent series resistance (ESR), it is also possible to predict the power losses from the spectrum of the energy storage current.

In addition the efficiency and ESR for the li-ion battery is measured according to draft standard ISO 12405-1 [12] and with a small scale straddle carrier laboratory drive. The purpose of the straddle carrier measurements is to analyze the correlation in efficiency and ESR between the fixed frequency calorimetric measurements and load current profile of an actual HWM.

Section II presents a description of the calorimetric measurement setup. Section III presents the results for the fixed frequency calorimetric measurements for both energy storages. Section IV presents the li-ion battery measurements according to draft standard ISO 12405-1 and Section V presents the li-ion battery measurements with the straddle carrier drive. Conclusions are drawn in Section VI.

II. THE CALORIMETRIC MEASUREMENT SETUP

A. *Balance Calorimeter Operation Principle*

A calorimeter is a thermally insulated container used to measure power losses of electrical components. The calorimeter used in this work is an air-cooled open-type balance calorimeter [9], [10]. Fig. 3 presents its operation principle and Fig. 4 the finished laboratory prototype.

The calorimeter consists of a 200 mm thick aluminum coated polyurethane measurement chamber, two temperature

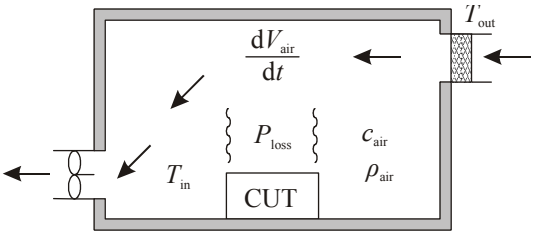

Figure 3. Balance calorimeter operation principle.

Figure 4. Balance calorimeter laboratory prototype.

transducers for measuring the inside and outside temperatures (T_{in}, T_{out}), a dc-fan in the outlet and an air-mass meter in the inlet.

During operation the component under test (CUT) dissipates heat to the measurement chamber, causing the temperature inside the calorimeter to rise. By generating a known constant air-flow dV_{air}/dt through the calorimeter, the power losses (P_{loss}) of the CUT can be calculated from the measured steady-state values of T_{in} and T_{out} [10]:

$$P_{loss} = \frac{dV_{air}}{dt} \cdot \rho_{air} \cdot c_{air} \cdot (T_{in} - T_{out}), \quad (1)$$

where c_{air} (= 1.005 kJ/kg K) is specific heat of air and ρ_{air} (= 1.205 kg/m^3) is air density.

Prior to the actual measurements of energy storage power losses, the calorimeter is calibrated with known electrical power supplied to a heat resistor. The calorimeter degree of filling and the distribution of air flow and temperature have an effect on the calorimeter performance. Thus, also the CUT is placed inside the calorimeter during calibration. The resulting calibration curves for the SC and li-ion battery are presented in Figs. 5a,b respectively. The P_{loss} for the CUTs

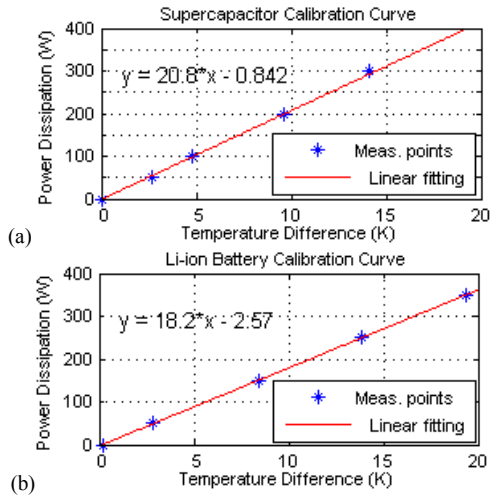

Figure 5. (a) Supercapacitor and (b) li-ion battery calibration curve.

are calculated from the equations for the calibration curves

$$P_{\text{loss,SC}} = 20.8 \cdot (T_{\text{in}} - T_{\text{out}}) - 0.842 \text{ (W)}, \quad \text{and} \quad P_{\text{loss,BAT}} = 18.2 \cdot (T_{\text{in}} - T_{\text{out}}) - 2.57 \text{ (W)}. \tag{2}$$

B. Test Setup for Efficiency Measurements

The test setup for measuring the energy storage P_{loss} is presented in Fig. 6. It consists of a 3-phase diode rectifier, a bidirectional dc-dc converter, a brake chopper and brake resistor R_{brake} in the system dc-link and the energy storage placed inside the calorimeter.

During energy storage charging, the system obtains its energy from the rectified 400 V supply grid. During energy storage discharge, energy is consumed in R_{brake} in order to maintain the dc-link voltage u_{dc} under an allowable level.

III. Calorimetric Measurement Results of the Energy Storages

A. Supercapacitor Measurements

The calorimetric measurements for the SC were performed at a total of eight operating points. The load currents examined were sinusoidal $I_{\text{es,rms}}$ = 50 A (0.33×I_{N}) and $I_{\text{es,rms}}$ = 84 A (0.56×I_{N}), with respective frequencies of 0.2 Hz, 1 Hz, 5 Hz and 10 Hz. During each measurement the SC voltage was kept at an average of $U_{\text{es,avg}}$ = 100 V, thus the average input-output power delivered to the SC is [11]

$$P_{\text{avg}} = \frac{2\sqrt{2} \cdot U_{\text{es,avg}} I_{\text{es,rms}}}{\pi}, \tag{3}$$

giving P_{avg} = 4500 W for $I_{\text{es,rms}}$ = 50 A and P_{avg} = 7560 W for $I_{\text{es,rms}}$ = 84 A respectively. Figs. 7a,b present an example of i_{es} and u_{es} waveforms within test point $I_{\text{es,rms}}$ = 84 A at 0.2 Hz frequency.

The measurement results are presented in Table II, where $\Delta T = T_{\text{in}} - T_{\text{out}}$, $R_{\text{ESR,SC}}$ the equivalent series resistance, and η_{SC} the charge-discharge efficiency of the SC. The calculation of $R_{\text{ESR,SC}}$ is performed as

$$R_{\text{ESR,SC}} = \frac{P_{\text{loss}} - P_{\text{vent}}}{I_{\text{es,rms}}^2}, \tag{4}$$

where P_{vent} is the auxiliary SC ventilation fan power of 13 W. The calculation of η_{SC} is performed as a function of P_{avg} and P_{loss} assuming equal efficiencies for charge and discharge operations:

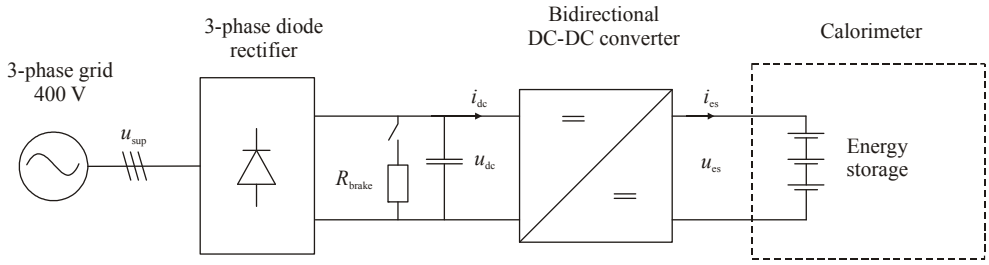

Figure 6. Test setup for energy storage efficiency measurements.

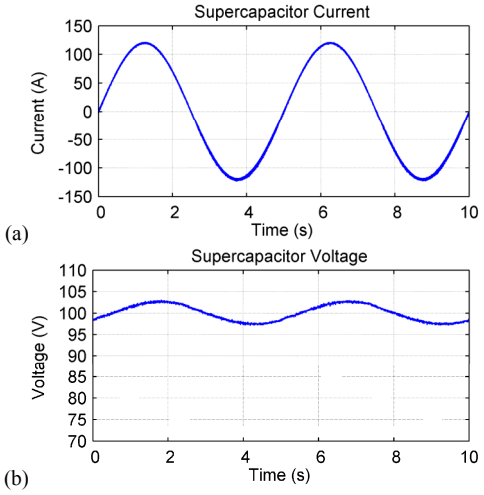

Figure 7. Supercapacitor (a) current and (b) voltage within test point $I_{\text{es,rms}}$ = 84 A and f = 0.2 Hz

TABLE II. Measurement Results for Supercapacitor Power Loss, R_{ESR}, and Efficiency

$I_{\text{es,rms}}$ (A)	f (Hz)	ΔT (K)	P_{loss} (W)	$R_{\text{ESR,SC}}$ (mΩ)	η_{SC} (%)
50	0.2	2.8	57	17.6	97.5
50	1	2.7	55	16.8	97.6
50	5	2.6	53	16.0	97.7
50	10	2.4	49	14.0	97.8
84	0.2	6.6	136	17.4	96.4
84	1	6.3	130	16.6	96.6
84	5	6.2	128	16.3	96.6
84	10	5.8	120	15.2	96.9

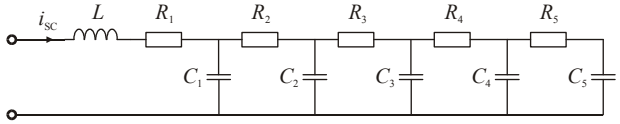

Figure 8. Multistage ladder model of the SC [13].

$$\eta_{SC} = \left(\frac{P_{avg} - P_{loss}}{P_{avg}} \right)^2 \cdot 100\,\% \cdot \quad (5)$$

The results indicate that η_{SC} varies between 96.4 % and 97.8 % and $R_{ESR,SC}$ between 14.0 mΩ and 17.6 mΩ. The increase in η_{SC} and decrease in $R_{ESR,SC}$ as the frequency increases can be explained e.g. through the multistage ladder model of Fig. 8, which describes the SC as a combination of multiple parallel RC-circuits [13]. The high frequency currents flow through the capacitances closer to the supply, while the lower frequency currents flow more deeply into the circuit. Hence, lower frequency currents encounter more resistance. Higher amplitude in the current leads to decrease in efficiency because P_{loss} is quadratically proportional to current ($P_{loss} = R_{ESR,SC} \times I_{es,rms}^2$). According to the manufacturer the value of $R_{ESR,SC}$ is 18 mΩ (Table I), which is close to the measured values with 0.2 Hz frequency.

B. *Li-ion Battery Measurements*

The calorimetric measurements for the li-ion battery were performed in a total of eight operating points. The battery was examined with sinusoidal 0.01 Hz, 0.1 Hz, 0.5 Hz, 1 Hz, 5 Hz and 10 Hz currents for $I_{es,rms} = 32$ A (0.36×C), and 0.1 Hz and 10 Hz for $I_{es,rms} = 64$ A (0.71×C). During each measurement the battery SOC was kept at 70 % and the average voltage was $U_{es,avg} = 99$ V. From (3) the average powers are $P_{avg} = 2850$ W for $I_{es,rms} = 32$ A and $P_{avg} = 5700$ W for $I_{es,rms} = 64$ A respectively.

The measurement results are presented in Table III, where η_{BAT} is the charge-discharge efficiency of the battery calculated from (5). $R_{ESR,BAT}$ is calculated from

TABLE III. MEASUREMENT RESULTS FOR LI-ION BATTERY POWER LOSS, R_{ESR}, AND EFFICIENCY

$I_{es,rms}$ (A)	f (Hz)	ΔT (K)	P_{loss} (W)	$R_{ESR,BAT}$ (mΩ)	η_{BAT} (%)
32	0.01	4.8	85	47.9	94.1
32	0.1	4.5	79	42.3	94.5
32	0.5	4.4	78	40.5	94.6
32	1	4.3	76	39.0	94.7
32	5	4.2	74	37.0	94.9
32	10	4.1	72	35.2	95.0
64	0.1	9.1	163	31.0	94.4
64	10	8.5	152	28.3	94.7

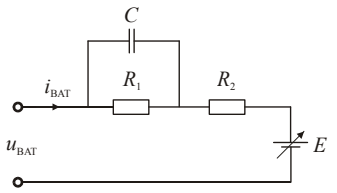

Figure 9. Dynamic li-ion battery model [14].

$$R_{ESR,BAT} = \frac{P_{loss} - P_{BMS}}{I_{es,rms}^2}, \quad (6)$$

where P_{BMS} is the power of the auxiliary battery management system of 36 W.

The measurement results indicate that η_{BAT} varies between 94.1 % and 95.0 % and $R_{ESR,BAT}$ between 28.3 mΩ and 47.9 mΩ. The increase in η_{BAT} and decrease in $R_{ESR,BAT}$ as the frequency increases can be explained e.g. through the dynamic li-ion battery model of Fig. 9 [14]. As the frequency of the battery current increases a larger portion of the current flows through the capacitance C, which is used to model the transient response of the battery voltage. Thus, higher frequency currents encounter less resistance than the lower frequency currents. Currents of higher amplitude yield higher battery operating temperature. In higher temperatures $R_{ESR,BAT}$ decreases [15], hence η_{BAT} degrades only slightly with 64 A currents in comparison with currents of 32 A.

IV. LI-ION BATTERY MEASUREMENTS WITH DRAFT STANDARD ISO/DIS 12405-1

In this section the li-ion battery ESR and energy efficiencies are determined from the draft standard ISO/DIS 12405-1, which proposes test specifications for li-ion traction battery systems for electrically propelled road vehicles [12]. Both measurements are carried out with the test setup of Fig. 6 except that the battery has been removed from the calorimeter. During the tests the average SOC of the battery is kept at 70 %.

A. *ESR Measurements*

Figs. 10a,b present the current and voltage profiles of the battery, used in the determination of its ESR. The test procedure is accomplished as follows: first the battery is discharged with maximum system current $I_{max} = 120$ A for 18 seconds, then kept unloaded for the next 40 seconds, after which it is charged for 10 seconds with $0.75 \times I_{max} = 90$ A,

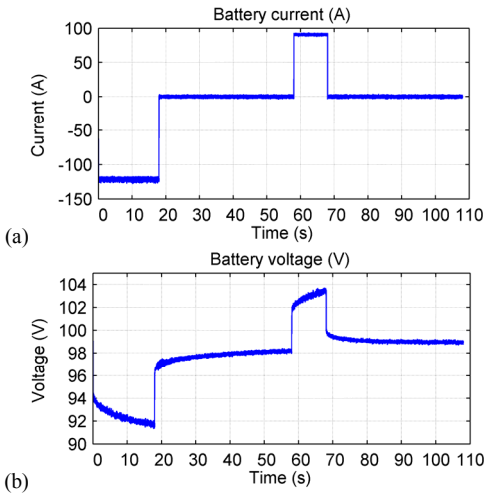

Figure 10. Battery (a) current and (b) voltage for determination of ESR.

TABLE IV. MEASUREMENT RESULTS FOR LI-ION BATTERY
R_{ESR} ACCORDING TO STANDARD ISO/DIS 12405-1

Time (s)	Voltage	Voltage value (V)	Current	Current value (A)		
0	U_0	99.1	I_0	0	**Formula**	$R_{ESR,BAT}$ (mΩ)
0.1	U_1	94.4	I_1	-120	$R_{0,1s,\,discharge} = (U_0 - U_1) / \lvert I_1 \rvert$	39.2
2	U_2	93.3	I_2	-120	$R_{2s,\,discharge} = (U_0 - U_2) / \lvert I_2 \rvert$	48.3
10	U_3	92.25	I_3	-120	$R_{10s,\,discharge} = (U_0 - U_3) / \lvert I_3 \rvert$	57.1
18	U_4	91.6	I_4	-120	$R_{18s,\,discharge} = (U_0 - U_4) / \lvert I_4 \rvert$	62.5
58	U_5	98.2	I_5	0	$R_{ESR,\,discharge} = (U_5 - U_4) / \lvert I_4 \rvert$	55.0
58.1	U_6	101.8	I_6	90	$R_{0,1s,\,charge} = \lvert (U_5 - U_6) \rvert / I_6$	40.0
60	U_7	102.5	I_7	90	$R_{2s,\,charge} = \lvert (U_5 - U_7) \rvert / I_7$	47.8
68	U_8	103.4	I_8	90	$R_{10s,\,charge} = \lvert (U_5 - U_8) \rvert / I_8$	57.8
108	U_9	98.95	I_9	0	$R_{ESR,\,charge} = \lvert (U_9 - U_8) \rvert / I_8$	49.4

and finally again kept unloaded for the last 40 seconds. The ESR for discharge operation is determined from the voltage rise during the first 40 second idle period (18 s – 58 s), and the ESR for charge operation is determined from the voltage drop of the last 40 second idle period (68 s – 108 s). In the measurements I_{max} is limited to 120 A, because this is the maximum continuous current of the dc-dc converter in the test setup.

The results for the ESR measurements are displayed in Table IV. For discharge operation $R_{ESR,BAT} = 55$ mΩ and for charge operation $R_{ESR,BAT} = 49.4$ mΩ. The results are in close correlation to the test point of 0.01 Hz and 32 A of the calorimetric measurements presented in Table III, which is the test point nearest to dc-current.

B. *Energy Efficiency Measurements*

Figs. 11a,b present the current and voltage profiles of the battery used in the determination of its energy efficiency. The current profile is now charge balanced. The test procedure is accomplished as follows: first the battery is discharged with $I_{max} = 120$ A for 12 seconds, then it is kept unloaded for 40 seconds, after which it is charged for 16 seconds with $0.75 \times I_{max} = 90$ A, and finally it is again kept unloaded for the last 40 seconds. The efficiency of the battery is calculated from

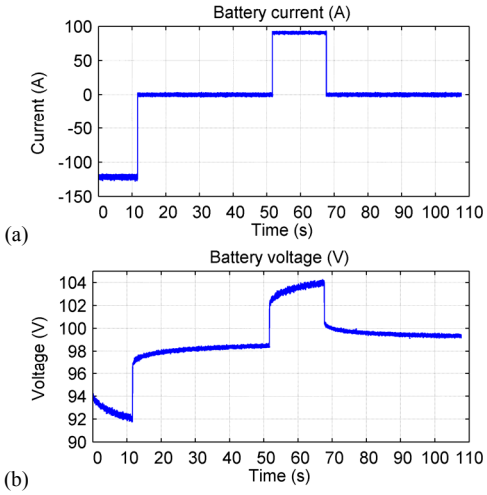

Figure 11. Battery (a) current and (b) voltage for determination of energy efficiency.

$$\eta_{BAT} = \frac{\int_{t_{start}}^{t_{end}} u_{BAT} \cdot i_{discharge} \cdot dt}{\int_{t_{start}}^{t_{end}} u_{BAT} \cdot i_{charge} \cdot dt} \times 100\ (\%). \quad (7)$$

The result of the efficiency calculation is $\eta_{BAT} = 90.07$ %, which is about 4 % – 5 % less than the calorimetric efficiencies in Table III. The discrepancy in the results can be explained through the higher current used in the standard procedure. As the current in the battery system increases, the power losses increase quadratically proportional to current and higher amplitude currents yield higher power losses in relation to the average input-output power of the battery. Carrying out the same experiment with lower current of $I_{max} = 90$ A and $0.75 \times I_{max} = 67.5$ A yields $\eta_{BAT} = 92.06$ %, which is closer to the efficiency measurements with the calorimeter.

V. LI-ION BATTERY EFFICIENCY MEASUREMENTS WITH LOAD PATTERN OF A STRADDLE CARRIER

In order to evaluate the performance of the li-ion battery with an actual load pattern of a HWM, a small scale laboratory drive of a hybridized straddle carrier has been built. Straddle carriers are used in port terminals for stacking and moving containers. Normally their transmission systems are diesel-hydraulic, with required peak power up to 300 kW. In this study the load pattern is reduced to 1/30 of the actual and the prototype is considered to model the power needed from the electrical part of a parallel hybridized straddle carrier.

The prototype is presented in Fig. 12. It consists of a 62 kW thyristor rectifier controlled DC load motor, which generates the desired torque T_{ref} to the shaft of the 11 kW

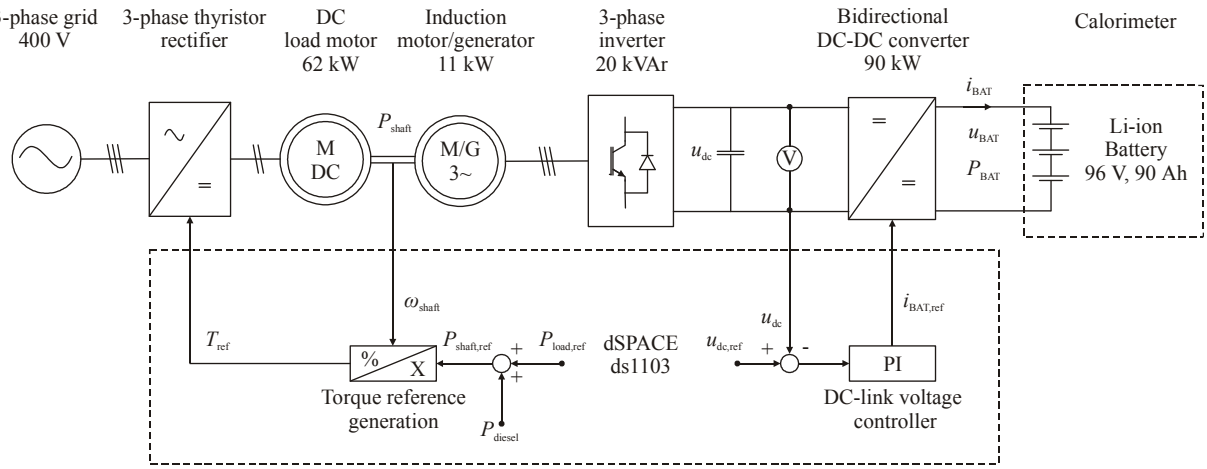

Figure 12. Laboratory drive for li-ion battery efficiency measurements with straddle carrier load pattern.

induction motor/generator, representing the electrical machine of the hybrid straddle carrier. The induction machine angular speed ω_{shaft} is controlled with a commercial 20 kVAr 3-phase inverter. The 90 kW bidirectional dc-dc converter is used to control u_{dc} with the current of the 96 V/ 90 Ah li-ion battery system.

The upper-level control of the prototype is performed with dSPACE ds1103 platform, including the dc-link voltage controller, torque reference generation and measurement signal acquisition. In order to perform long-term calorimetric measurements, the system is controlled in such a way that the SOC of the battery remains constant after each load cycle. This means that the average power of the load cycle and the power losses of the induction machine, power electronics and the li-ion battery are compensated with an imaginary diesel motor P_{diesel} coupled to the same shaft with the induction machine. I.e. P_{diesel} is added to $P_{load,ref}$, which equals $P_{shaft,ref}$.

Figs. 13a–e present measurement results for P_{shaft} (blue) and $P_{shaft,ref}$ (red), battery power P_{BAT}, i_{BAT}, battery SOC, and a spectrum of i_{BAT} during one working cycle of 144 seconds. Positive power or current states for regenerative operation of the straddle carrier, i.e. braking or load lowering movements. Negative values indicate acceleration or load lifting operations respectively.

The peak power of the induction machine (Fig. 13a) is 18 kW. It has an offset of 2.82 kW, which is needed from the imaginary diesel motor to maintain the battery SOC at constant 70 % (Fig. 13d) under long-term operation. During one load cycle the battery experiences an average input-output power of $P_{BAT,avg}$ = 2665 W (Fig. 13b). The rms value

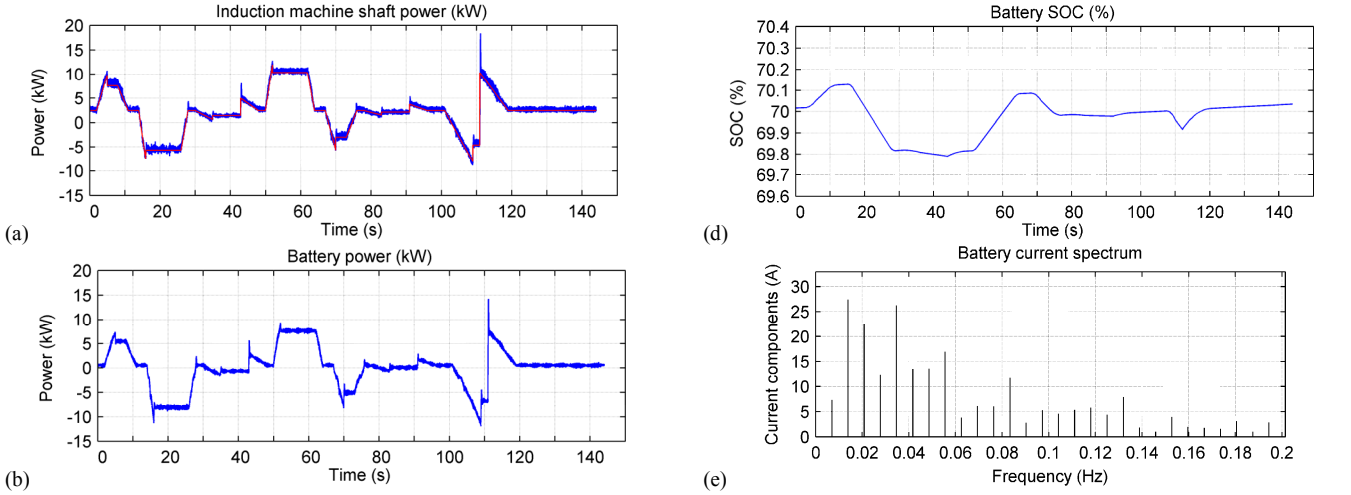

Figure 13. Measured waveforms of straddle carrier laboratory drive. (a) Induction motor shaft power, (b) battery power, (c) battery current, (d) battery SOC, and (e) battery current spectrum.

of the battery current (Fig. 13c) is $i_{BAT,rms} = 40.2$ A. The battery current spectrum of Fig. 13e indicates that the largest current components occur at frequencies of 0.01 – 0.05 Hz, respectively.

A long-term calorimetric measurement was performed for the battery, and the result is presented in Table V. During the measurement the temperature difference of the calorimeter rose to 5.7 K, meaning an average power loss of 101 W. From (6) $R_{ESR,BAT} = 40.2$ mΩ with $P_{BMS} = 36$ W. The efficiency of the battery, calculated from (5) is $\eta_{BAT} = 92.6$ %.

Comparing the results with the fixed frequency measurements of Table III indicates that η_{BAT} is 1.5 % smaller than e.g. in the measurement point of $I_{es,rms} = 32$ A and $f = 0.01$ Hz. The efficiency decreases because i_{BAT} contains long duration current peaks of higher amplitude in comparison with the fixed frequency measurements. This means higher $I_{es,rms}$ and, hence higher P_{loss} in proportion to P_{avg}. The value of $R_{ESR,BAT}$ is in correlation with the fixed frequency measurements.

VI. Conclusion

This paper presented efficiency and ESR measurements for a Maxwell BMOD0063 P125 V/63 F heavy duty SC module and a K2 96 V/ 90 Ah li-ion battery system comprising of 30 pcs of LFP300HES Energy Modules. The aim was to study if the frequency of the energy storage current had a dramatic effect on the energy storage efficiency. A calorimetric test setup was built in order to obtain accurate measurement results. In addition the li-ion battery efficiency and ESR was measured according to draft standard ISO 12405-1 and with a small scale straddle carrier laboratory drive representing a load pattern of an actual HWM.

The fixed frequency calorimetric measurements indicate that in both energy storages the efficiency increases as the frequency increases, but overall the frequency has a maximum of 1 % effect on the efficiencies. The efficiency for the SC varies between 96.4 % and 97.8 % and the efficiency for the li-ion battery between 94.1 % and 95.0 %. The li-ion battery standard measurements are in correlation with the calorimetric measurements for the battery ESR, but the higher amplitude currents in the standard procedure lead to decreased efficiency in comparison with the calorimetric measurements. The battery current of the straddle carrier drive also contains current peaks of high amplitudes, which reduces the efficiency compared with the calorimetric measurements.

Overall the results predict that the efficiency of the SC is approximately 3 % better than that of the li-ion battery system. Hence, in parallel SC and li-ion battery energy storage systems the control of power flow should be arranged so that the SC is utilized as much as possible.

TABLE V. Li-ion Battery Power Loss, R_{ESR}, and Efficiency During Load Cycle of Straddle Carrier

$I_{es,rms}$ (A)	f (Hz)	ΔT (K)	P_{loss} (W)	$R_{ESR,BAT}$ (mΩ)	η_{BAT} (%)
40.2	0.01…0.05	5.7	101	40.2	92.6

References

[1] A. Emadi, Handbook of automotive power electronics and motor drives, Taylor & Francis, Boca Raton, 2005.

[2] C. C. Chan, "The state of the art of electric, hybrid, and fuel cell vehicles," Proceedings of the IEEE, vol. 95, no. 4, pp. 704-718, Apr. 2007.

[3] P. Immonen, L. Laurila, M. Rilla, and J. Pyrhönen, "Modelling and simulation of a parallel hybrid drive system for mobile work machines," in proc. IEEE EUROCON '09, 2009, pp. 867-872.

[4] S. D.Lukic, J. Cao, R. C. Bansal, F. Rodriguez, and A. Emadi, "Energy storage systems for automotive applications", IEEE Transactions on Industrial Electronics, vol. 55, no. 6, pp. 2258-2267, Jun. 2008

[5] A. Virtanen, and H. Tuusa, "Power compensator for high power fluctuating loads with a supercapacitor bank energy storage," in proc. IEEE 2008 International Conference on Power and Energy, 2008, pp. 977-982.

[6] S. M. Lukic, S. G. Wirasingha, F. Rodriguez, J. Cao, and A. Emadi, "Power management of an ultracapacitor/battery hybrid energy storage system in an HEV," in proc. IEEE 2006 Vehicle Power and Propulsion Conference, 2006, pp. 1-6.

[7] F. S. Garcia, A. A. Ferreira, and J. A. Pomilio, "Control strategy for battery-ultracapacitor hybrid energy storage system," in proc. IEEE 2009 Applied Power Electronics Conference, 2009, pp. 826-832.

[8] A. L. Allegre, A. Bouscayrol, and R. Trigui, "Influence of control strategies on battery/supercapacitor hybrid energy storage systems for traction applications," in proc. IEEE 2009 Vehicle Power and Propulsion Conference, 2009, pp. 213-220.

[9] D. R. Turner, K. J. Binns, and B. N. Shamsadeen, "Accurate measurement of induction motor losses using balance calorimeter," IEE Proceedings–B, vol. 138, no. 5, pp. 233-242, Sept. 1991.

[10] C. Xiao, G. Chen, and W. G. H. Odendaal, "Overview of power loss measurement techniques in power electronics systems," IEEE Transactions on Industry Applications, vol. 43, no. 3, pp. 657-664, May/Jun. 2007.

[11] N. Mohan, T. M. Undeland, and W. P. Robbins, Power electronics: converters, applications and design, John Wiley & Sons, Hoboken, NJ, USA, 2003.

[12] ISO/DIS 12405-1, Electrically propelled road vehicles – Test specification for lithium-Ion traction battery packs and systems – Part 1: High power applications, 2009.

[13] R. A. Douga, L. Gao, S. Liu, "Ultracapacitor model with automatic order selection and capacity scaling for dynamic system simulation", Journal of Power Sources, vol. 126, no. 1–2, pp. 250–257, Feb. 2004.

[14] L. Gao, S. Liu, R. A. Dougal, "A dynamic lithium-ion battery model for system simulation", IEEE Transactions on Components and Packaging Technologies, vol. 25, no. 3, pp. 495–505, Sept. 2002.

[15] J. Kim, S. Lee, B. Cho, "The state of charge estimation employing empirical parametrs measurements for various temperatures", in proc. IEEE 2009 Power Electronics and Motion Conference, 2009, pp. 939-944